

1 This manuscript is a non-peer reviewed preprint submitted to EarthArXiv. This manuscript has
2 been submitted for publication in Journal of Hydrometeorology.

3 **How Will Precipitation Characteristics Associated with Tropical Cyclones in**
4 **Diverse Synoptic Environments Respond to Climate Change?**

5 Katherine E. Hollinger Beatty^a, Gary M. Lackmann^a, and Jared H. Bowden^{a,b}

6 ^a*North Carolina State University, Raleigh, North Carolina*

7 ^b*North Carolina State Climate Office, Raleigh, North Carolina*

8 *Corresponding author:* Katherine E. Hollinger Beatty, kehollin@ncsu.edu

9 ABSTRACT: Landfalling tropical cyclones (TCs) can produce large rainfall totals which lead
10 to devastating flooding, loss of life, and significant damage to infrastructure. Here we focus
11 on three North Atlantic TCs that impacted the southeastern United States: Hurricanes Floyd
12 (1999), Matthew (2016), and Florence (2018). While these storms were impactful when they
13 occurred, how might the impacts of similar systems change in a future climate? Many studies
14 have examined future changes in TC precipitation, however few have considered changes owing
15 to differences in the synoptic environment during landfall. We address these questions using a
16 Pseudo-Global Warming (PGW) approach and ensembles of convection-allowing numerical model
17 simulations. With this method, we compare future changes in precipitation characteristics such
18 as accumulated rainfall, and rain rate frequency and distribution to assess how they differ as a
19 function of synoptic environment. Hurricanes Matthew and Floyd, which have more synoptic-
20 scale forcing for ascent while over our study region, exhibit higher average rain rates in the present
21 and future than the more tropical Hurricane Florence, but Florence has the largest increases in
22 rain rates ($34 \pm 12\%$ versus $23 \pm 9\%$ and $21 \pm 6\%$ for Hurricanes Matthew and Floyd, respectively).
23 When we consider accumulated precipitation, Hurricanes Matthew and Floyd have larger areal
24 increases in precipitation greater than 250 mm than Florence ($17600 \pm 800km^2$ and $22400 \pm 400km^2$
25 versus $9800 \pm 500km^2$). These results point to the potential for future TCs in synoptically forced
26 environments to have larger spatial footprints of accumulated precipitation but smaller increases
27 in rain rate than non-synoptic storms, especially when considering overland precipitation.

28 SIGNIFICANCE STATEMENT: Many previous studies demonstrate that tropical cyclone (TC)
29 precipitation will increase in a warmer climate, but few studies consider how TC precipitation
30 responds to climate change as a function of the accompanying weather pattern. This study aims
31 to identify how rainfall from three Atlantic TCs in distinct weather patterns would look if they
32 occurred in a warmer environment. By understanding how TC rainfall for a diverse set of weather
33 patterns responds to warming, we can make recommendations for infrastructure and community
34 preparation to increase readiness for future storms, with the ultimate goal of minimizing future
35 damage and loss of life. These simulations specifically are being applied to better understand future
36 flooding risks for long-lived transportation infrastructure within eastern North Carolina.

37 1. Introduction

38 As tropical cyclones (TCs) affect coastlines and communities, they can cause substantial structural
39 damage and loss of life. One of the largest contributors to these impacts is heavy precipitation
40 and subsequent flooding or flash flooding. Rappaport (2014) found that for historical Atlantic
41 TCs affecting the United States (US), approximately one quarter of the fatalities were a result of
42 rain-induced flooding. When considering the frequency of fatalities, they found that nearly half
43 of the TCs that resulted in at least one US fatality had a fatality due to rain-induced flooding
44 (Rappaport 2014). This is especially true in the US states of North and South Carolina, where in
45 the last 10 years, flooding from storms such as Hurricane Florence (2018) and Hurricane Matthew
46 (2016) resulted in dozens of fatalities, multiple road washouts, and the closure of multiple major
47 state and interstate highways (Stewart 2017; Stewart and Berg 2019).

48 It is clear that heavy rainfall from TCs has caused devastating impacts historically, and many
49 previous studies have also examined how precipitation and its associated impacts may change as the
50 climate warms. Per the IPCC AR6 Report (Seneviratne et al. 2023), there is high confidence that
51 TC rain rates will increase in the future; for TCs passing over or near North Carolina, specifically,
52 Kunkel et al. (2020) report that the heavy precipitation associated with them is very likely to
53 increase. Of the numerous studies that have analyzed TC precipitation changes with climate
54 change, a central finding is an increase in rain rates that either follows, or in some studies exceeds,
55 the Clausius-Clapeyron scaling ($\sim 7\%$ increase per degree Celsius of warming) (Knutson and Tuleya
56 2004; Hill and Lackmann 2011; Knutson et al. 2015). Knutson et al. (2020), in reviewing multiple

57 studies, found that near-storm TC rain rates globally increase by a median value of 14% with a
58 range from 6 to 22%, with slight variations by ocean basin; studies of the North Atlantic TCs show
59 a median increase of ~16% (Knutson et al. 2020). While rainfall characteristics for TCs over water
60 are important to understand, most of the societal impacts from TC rainfall, such as flooding, road
61 washouts, and fatalities, occur once the storm is over land. A smaller portion of TC rainfall studies
62 have focused explicitly on these landfalling/over-land changes in precipitation (Wright et al. 2015;
63 Liu et al. 2018; Stansfield et al. 2020; Knutson et al. 2022), and their results are consistent in
64 showing increased average post-landfall TC rain rates. While these studies provide useful insight,
65 one limitation of many such studies is their use of lower-resolution simulations and datasets, and
66 methods that do not capture the full extent of changes in TC intensity or precipitation (e.g. Liu
67 et al. 2018; Stansfield et al. 2020).

68 When TCs make landfall or interact with land, especially once they enter the mid-latitudes, they
69 often undergo the process of extratropical transition (ET) and some of their tropical features are
70 replaced with extratropical characteristics. This phenomenon has been studied extensively (e.g.
71 Jones et al. 2003; Evans et al. 2017; Keller et al. 2019), and its correlative changes in rainfall
72 characteristics, including a shift of the heaviest precipitation into the northwest quadrant of the
73 storm, are well understood (e.g. Atallah et al. 2007). How these extratropical transitioning storms
74 will change with climate warming has also received recent attention (e.g. Liu et al. 2017; Michaelis
75 and Lackmann 2019; Bieli et al. 2020; Liu et al. 2020; Michaelis and Lackmann 2021; Jung
76 and Lackmann 2021, 2023), however only a few studies have focused specifically on rainfall,
77 and how ET TC rainfall changes compare with non-ET TCs that are more tropical in character
78 (e.g. Liu et al. 2018). Another factor that coincides with TCs in various life-cycle phases is the
79 different synoptic environments within which they exist, and how the rainfall produced by TCs in
80 distinct environments may change as the climate warms. To the authors' knowledge, this aspect,
81 specifically, has received very limited attention.

82 Our goal in this paper is to focus on how TC rainfall over land changes with climate warming, and
83 how these changes differ for TCs at various stages of their life cycle (tropical versus extratropical-
84 transitioning) and in differing synoptic environments. To answer these questions, we analyze
85 three synoptically diverse TCs that produced prolific rainfall (greater than 400 mm maximum
86 accumulated rainfall) over the United States in North and South Carolina, specifically: Hurricanes

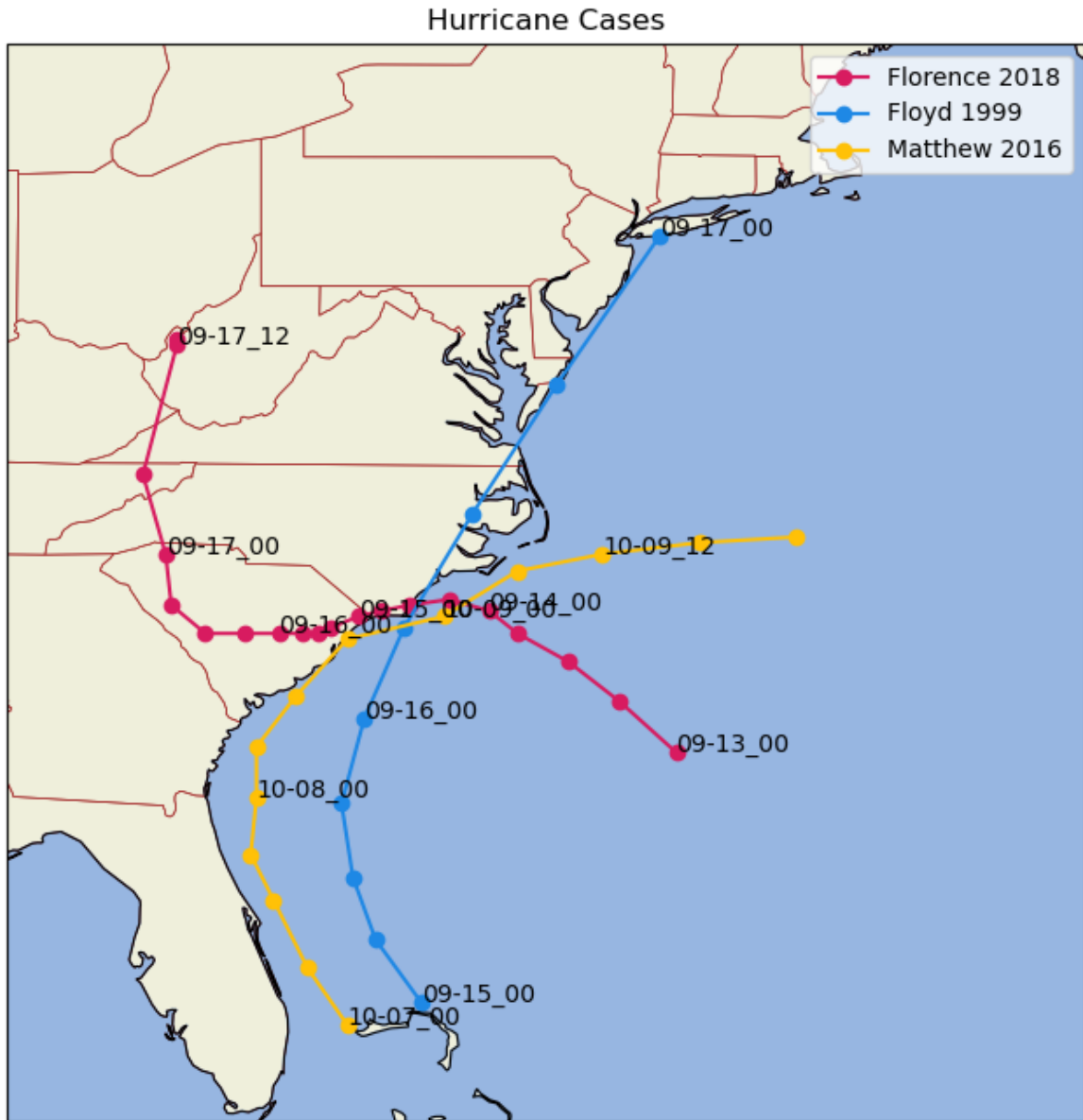
87 Floyd (1999), Matthew (2016), and Florence (2018). We conducted ensemble simulations of
88 these three storms at high-resolution using the Weather Research and Forecasting (WRF) model
89 (Skamarock et al. 2019) for present-day conditions, and then in a future environment using a
90 Pseudo-Global Warming (PGW, a.k.a. physical climate storyline) approach (Schär et al. 1996; Frei
91 et al. 1998; Kimura and Kitoh 2007; Sato et al. 2007; Baulenas et al. 2023). This approach has
92 proven successful for various precipitation-producing weather phenomena previously, including
93 individual TCs (e.g. Lackmann 2015; Jung and Lackmann 2019; Carroll-Smith et al. 2020; Reed
94 et al. 2020), full TC seasons (e.g. Mallard et al. 2013a,b; Gutmann et al. 2018), and smaller-scale
95 convective systems (e.g. Lackmann 2013; Trapp and Hoogewind 2016; Dougherty and Rasmussen
96 2020; Dougherty et al. 2023).

97 This paper focuses on how the precipitation characteristics for these storms responds to climate
98 change. Section two here focuses on data and methods, followed by an evaluation of the simu-
99 lations with respect to observations in section three. Section four discusses specific changes in
100 precipitation characteristics for these storms, including changes in accumulated precipitation, rain
101 rate distribution, and rain rate spatial extent, followed by conclusions and discussion in section
102 five.

103 **2. Data and Methods**

104 *a. Case selection and overview*

105 For this study, we chose to analyze Western North Atlantic Hurricanes Floyd (1999), Matthew
106 (2016), and Florence (2018), with a specific focus on the portion of their lifetime as they approached
107 and impacted the US states of North and South Carolina. We selected these cases on the basis
108 of their contrasting synoptic environments, which influenced the track (Fig. 1), structure, and
109 evolution of these systems: one remained more purely tropical (Florence), one became strongly
110 extratropical as it completed ET (Floyd), and one was weakly extratropical and barely made landfall
111 in the affected states, while not fully completing ET (Matthew). These cases are also of interest to
112 the North Carolina Department of Transportation because they each resulted in extensive disruption
113 and damage to transportation infrastructure, in addition to being responsible for numerous fatalities.
114 Hurricanes Matthew and Florence in particular resulted in the closure of multiple major interstate



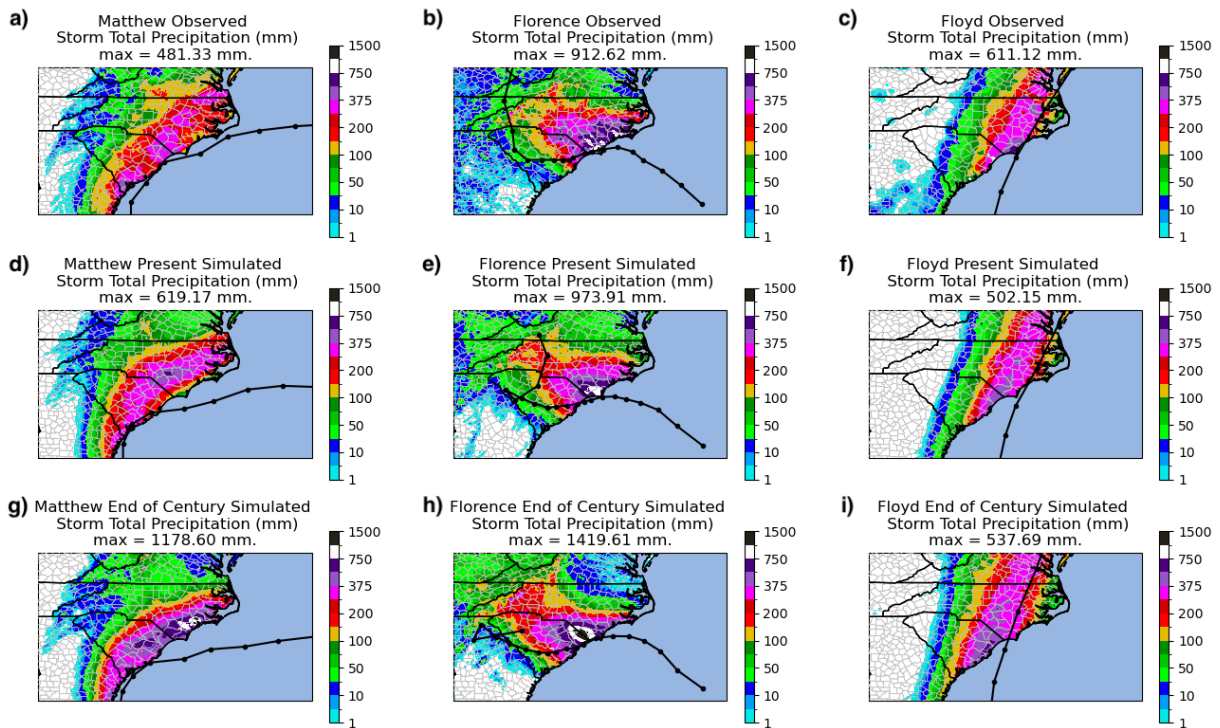
117 Figure 1. Observed National Hurricane Center (NHC) second-generation hurricane database (HURDAT2;
 118 Landsea and Franklin 2013) storm tracks of Hurricanes Matthew (2016), Florence (2018), and Floyd (1999)
 119 during the portion of their life cycles when they were approaching or affecting the study area. Numbers correspond
 120 to month-day-hour in UTC.

115 highways. While these storms do not represent all possible storm evolutions that could impact this
 116 region, they provide diverse synoptic representations of impactful storms that affected this region.

121 Hurricane Floyd made landfall in North Carolina near Cape Fear at 0630 UTC on 16 September
122 1999 as a category two hurricane on the Saffir-Simpson scale (Pasch et al. 1999). In the roughly 24
123 hours that Floyd directly affected the Carolinas, it produced large regions of 250-400 mm (10-15
124 inches) of rain, with a peak value of 611 mm (24.06 inches) reported near the coast in Wilmington,
125 NC (Pasch et al. 1999, Fig. 2c). This rainfall was likely enhanced by Floyd's interactions with
126 an approaching cold front and upper-tropospheric trough (Atallah and Bosart 2003). As Floyd
127 approached and moved across North Carolina, its translation speed increased. It then turned north-
128 northeast and encountered an environment with increased south-southeasterly shear, and began to
129 acquire extratropical characteristics which classified it as an asymmetric warm core system (Fig.
130 3c). Floyd moved up the East Coast and continued to interact with the front, producing rainfall
131 totals greater than 250 mm across Maryland, Delaware, and New Jersey and record breaking rainfall
132 in Philadelphia (Pasch et al. 1999). It was classified as a frontal low by the time it reached Maine,
133 thus completing its extratropical transition. Atallah and Bosart (2003) and Colle (2003) give more
134 thorough analyses of Hurricane Floyd's life cycle and extratropical transition along the US East
135 Coast.

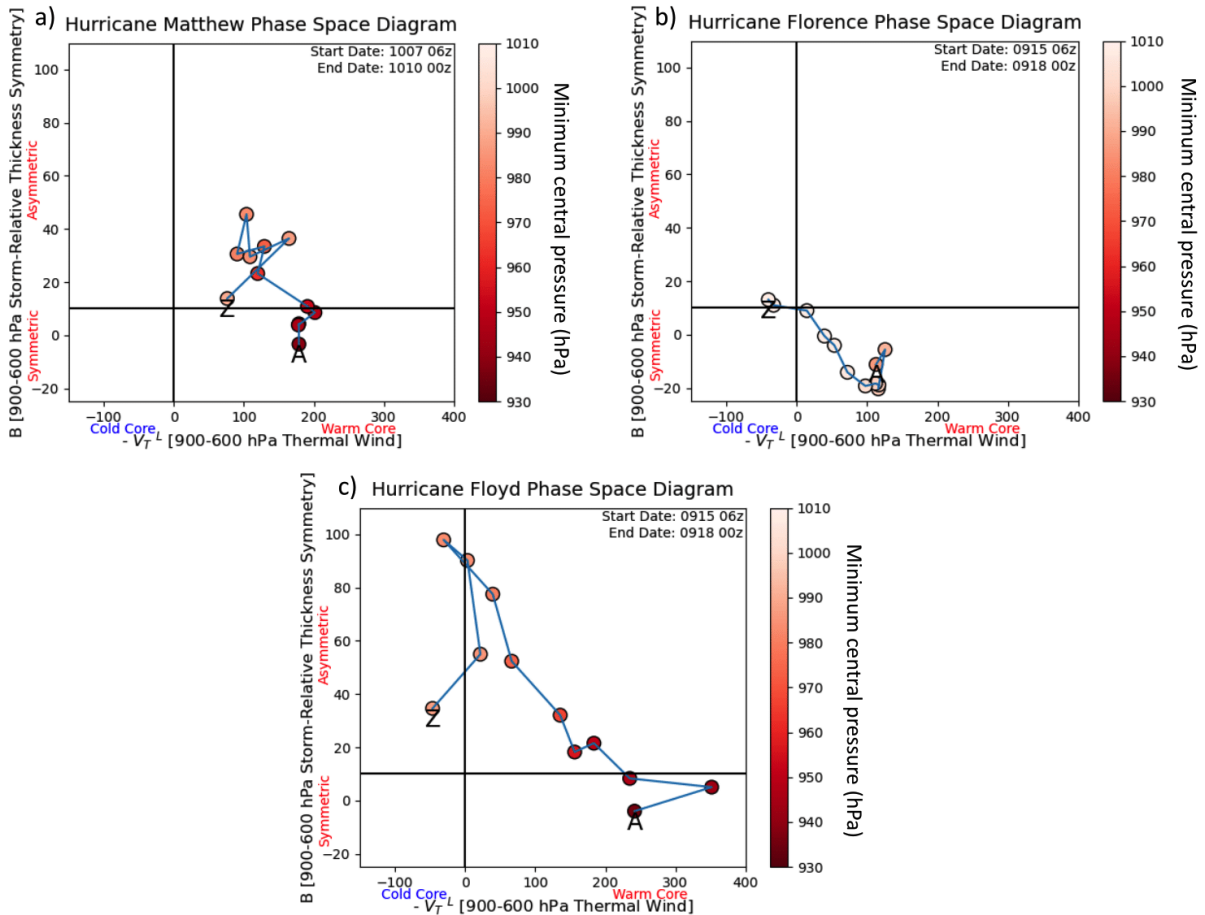
144 Hurricane Matthew briefly made landfall in northeastern South Carolina near McClellanville
145 around 1500 UTC 8 October 2016 before making a sharp eastward turn as it interacted with an
146 eroding subtropical high and an approaching mid-latitude trough (Stewart 2017). Because of the
147 interactions with the approaching trough and an existing front over North Carolina, Hurricane
148 Matthew's cloud and precipitation shield was shifted to the northwest of the storm center, resulting
149 in large regions of greater than 250 mm (10 inches) of rain over central and eastern NC, with a
150 maximum measured value of 481 mm (18.95 inches) reported near Evergreen, NC (Stewart 2017,
151 Fig. 2a). This left-of-track precipitation shield is similar to what was seen with Hurricane Floyd,
152 though the tracks for these two storms differed substantially (Figs.1, 2a,c). It is also indicative of
153 a shift to an asymmetric warm-core system instead of a more tropical symmetric warm core TC
154 (Fig. 3a). After impacting North Carolina, Matthew continued to move eastward over the Atlantic
155 before fully losing its tropical characteristics around 1200 UTC 9 October, then merging with the
156 frontal system by 0000 UTC 10 October (Stewart 2017).

157 Hurricane Florence made landfall near Wrightsville Beach, NC as a category one hurricane
158 around 1115 UTC on 14 September 2018 (Stewart and Berg 2019). As it approached North



136 Figure 2. Precipitation and track summary, panels (a)-(c): Black line is observed NHC best track for Hurricanes
 137 (a) Matthew (2016), (b) Florence (2018), and (c) Floyd (1999) with storm total precipitation (shaded, mm as in
 138 legend at right). Observed precipitation for Hurricanes Matthew and Florence is Stage IV and for Hurricane Floyd
 139 is Livneh daily CONUS near-surface gridded precipitation provided by the NOAA PSL (Livneh et al. 2013).
 140 Panels (d)-(f): Simulated ensemble mean track and probability matched mean total accumulated precipitation
 141 (mm) from WRF model simulations of Hurricanes (d) Matthew, (e) Florence, and (f) Floyd. Panels (g)-(i):
 142 ensemble mean track and probability matched mean total accumulated precipitation (mm) from future WRF
 143 model runs of Hurricanes (g) Matthew, (h) Florence, and (i) Floyd.

159 Carolina from the east-southeast, its steering flow weakened which caused a subsequent decrease
 160 in translation speed. This slow translation speed allowed for continued access to the warm Gulf
 161 Stream waters off the coast of the Carolinas, resulting in multiple rain bands passing over the same
 162 parts of southeastern North Carolina and prolonging the duration of heavy precipitation. There
 163 were large regions of greater than 250 mm (10 inches) of rainfall in central and southeastern North
 164 Carolina, with a smaller region of greater than 500 mm (20 inches) over far southeastern NC, and
 165 a localized region of greater than 750 mm (30 inches) from the persistent rain bands; the peak
 166 rainfall reported was 912 mm (35.93 inches) near Elizabethtown, NC (Stewart and Berg 2019, Fig.



171 Figure 3. Cyclone phase space (CPS) diagrams of thickness symmetry versus lower-tropospheric thermal wind
 172 for Hurricanes Matthew (a), Florence (b), and Floyd (c). Values are plotted every 6 hours with color shading to
 173 indicate the minimum central pressure (hPa) for each storm as in legend at right. The letters A and Z represent
 174 the beginning and end of time window for each storm, respectively.

167 2b). Because of its slow translation speed, Florence continued to produce heavy rainfall over some
 168 parts of central and eastern North Carolina for over 72 hours, and maintained symmetric warm
 169 core tropical characteristics until it reached West Virginia around 1200 UTC 17 September when
 170 it was officially considered extratropical (Stewart and Berg 2019, Fig. 3b).

175 *b. Model configuration*

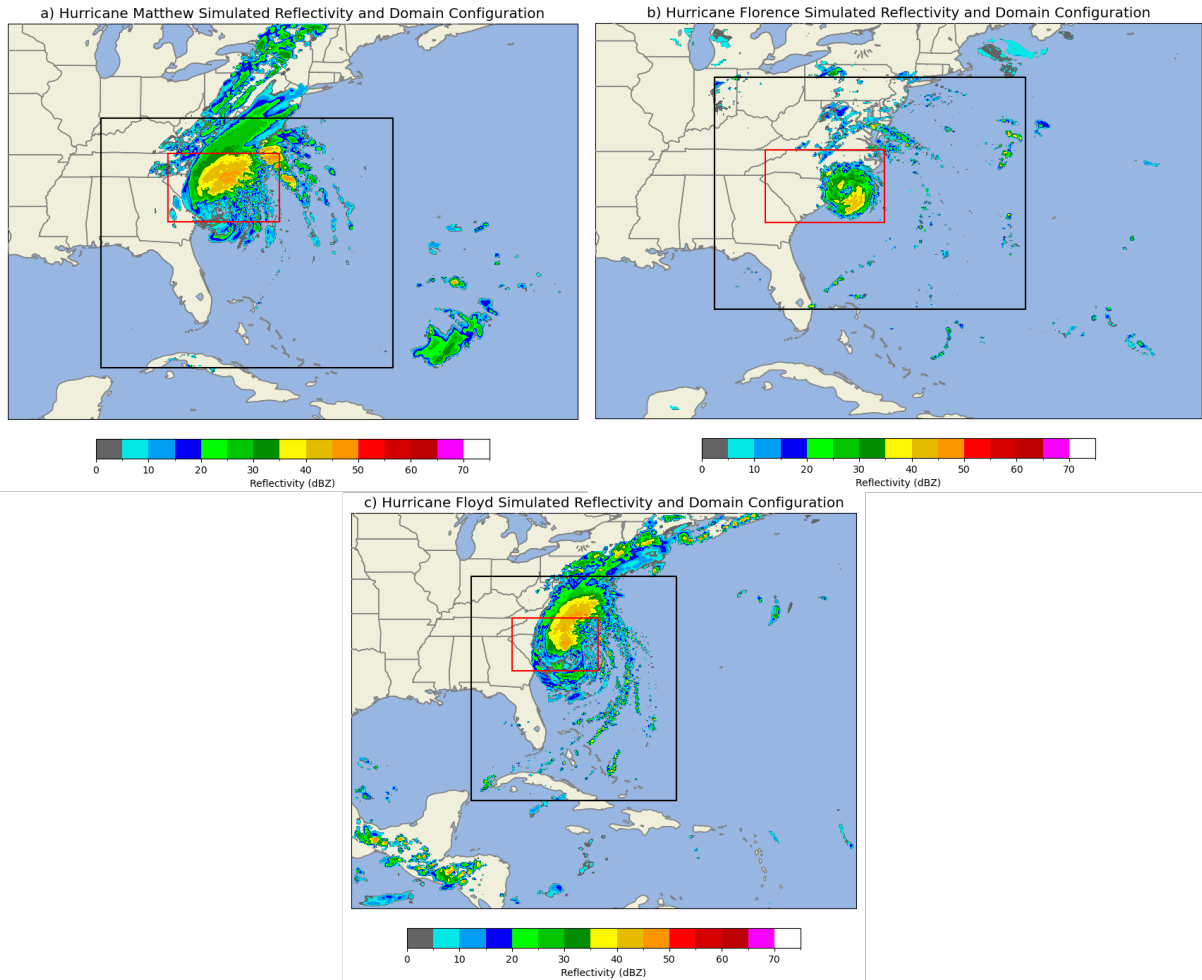
176 We simulated each storm using the Weather Research and Forecasting (WRF) Model version
 177 4.2.2 (Skamarock et al. 2019). We experimented with different initialization (and lateral boundary

198 Table 1. Physics choices used for each ensemble member for WRF simulations. Hurricanes Florence and
 199 Floyd used all 7 members, while Hurricane Matthew only used the first 6.

	<i>Member1</i>	<i>Member2</i>	<i>Member3</i>	<i>Member4</i>	<i>Member5</i>	<i>Member6</i>	<i>Member7</i>
Microphysics	Thompson	WSM6	Thompson	Goddard	P3	WDM6	WDM7
Cumulus (domain 1 only)	Tiedtke	Tiedtke	BMJ	Tiedtke	Tiedtke	Tiedtke	Tiedtke
PBL	YSU	YSU	MYJ	YSU	YSU	YSU	YSU
Surface-layer	MM5	MM5	Eta	MM5	MM5	MM5	MM5

178 condition) datasets to identify which yielded simulations that most closely matched observations.
 179 We decided to initialize Hurricane Matthew with the 0.25° ERA5 dataset (Hersbach et al. 2020)
 180 and simulated the period from 00 UTC 06 October until 00 UTC 10 October 2016. For Hurricane
 181 Florence, we used the 0.25° Final Global Data Assimilation System (GDAS/FNL) dataset (National
 182 Centers for Environmental Prediction, National Weather Service, NOAA, U.S. Department of
 183 Commerce 2015) and simulated the period from 00 UTC 13 September until 18 UTC 17 September
 184 2018. For Hurricane Floyd, we used the 0.5° Climate Forecast System (CFSR) (Saha et al. 2010)
 185 dataset and simulated the period from 00 UTC 14 September to 00 UTC 17 September 1999. We
 186 ran a mini-ensemble of simulations for each storm based on varying physical parameterizations;
 187 this ensures that results are not particular to a specific set of model physics choices, and offers a
 188 more robust solution, while also providing ensemble statistics and information about uncertainty.
 189 For Hurricane Matthew, we ran six ensemble members while for Hurricanes Florence and Floyd we
 190 ran seven ensemble members (Table 1). Each of our storms had a parent domain with 12-km grid
 191 spacing and a stationary inner nest with 4-km grid spacing (Fig. 4); we used two-way nesting so
 192 that information from the high-resolution domain was fed back to the parent domain. The physics
 193 choices for each ensemble member are the same for both the parent domain and the nest, except
 194 for the cumulus scheme which was turned off for the nested domain given the higher resolution.
 195 All ensemble members also used the ocean mixed layer model to adjust for the cold wakes behind
 196 the TCs and the “isftcflx” in WRF is set to the Donelan/Garret formulation to adjust the overwater
 197 surface flux exchange coefficients at high wind speed (Donelan et al. 2004).

205 Given that the focus of our study is over-land precipitation and how it responds to climate
 206 change, it is imperative that our present and future storms overlap as much as possible; as such, the



200 Figure 4. WRF domain configurations for Hurricanes Matthew (a), Florence (b), and Floyd (c). The full image
 201 is the 12 km parent domain and the black box is the 4 km nested domain. The red box represents the averaging
 202 domain used when considering rainfall changes over the Carolinas. The simulated reflectivity is valid at 18z 08
 203 October, 12z 14 September, and 06z 16 September for Hurricanes Matthew, Florence, and Floyd, respectively,
 204 and at 12km and 4km resolution in each respective domain.

207 simulation verification metric we emphasize is the accumulated storm-total rainfall. To maintain
 208 track similarity and more similar accumulated rainfall distributions, we used spectral nudging for
 209 each ensemble member for Hurricanes Matthew and Florence (Waldron et al. 1996; von Storch
 210 et al. 2000; Bowden et al. 2012; Otte et al. 2012). Our specific configuration included nudging of
 211 only the winds above the boundary layer (model level 10 which corresponds to ~800 hPa base state
 212 pressure) at wavenumbers three and smaller on the parent domain; this corresponds to features at

213 spatial scales on the order of 1000 km and greater. We did not nudge geopotential, temperature,
214 or water vapor, and we did not nudge any variables in the nested domain. Our goal with this
215 configuration was to nudge just the large-scale pattern to the reanalysis data to allow the steering
216 flow to be similar in the present and future environments while still allowing the storm-scale
217 features to freely evolve, and to maintain the warmer thermodynamic conditions for the future
218 simulations. While we tested nudging with Hurricane Floyd, we ultimately did not use it because
219 the tracks were sufficiently similar to observations without nudging (Fig. 5c,f).

220 In order to compensate for large underestimations in TC intensity in available reanalyses for
221 Hurricane Floyd, we initialized simulations of that storm with a synthetic vortex, following Nolan
222 et al. (2021). This method allowed the intensity of the storm to be closer to observations relative
223 to simulations initialized with the reanalysis alone. The synthetic vortex was especially useful for
224 Hurricane Floyd, but was not used for Matthew or Florence. For Florence, the intensity, track, and
225 precipitation distribution using reanalysis alone aligned well with the observations (discussed in
226 section 3), so the vortex was not needed. For Matthew, the precipitation distribution and the tracks
227 were close to observations without the synthetic vortex, however the intensity was substantially
228 weaker than observed. To attempt to resolve this disparity, we tested one ensemble member using
229 the synthetic vortex, and while the intensity improved, the storm track and precipitation distribution
230 were more poorly represented (not shown). Given the purpose of these simulations for assessing
231 transportation risk to hurricane precipitation in a warmer climate, the non-synthetic vortex Matthew
232 runs were sufficient. Throughout the model configuration process, all simulations were compared
233 with their respective storm's observed track, intensity, and precipitation distribution to assess their
234 validity, which will be discussed in more detail in section three.

235 *c. Future climate simulations*

236 To investigate how these storms would differ in a future thermodynamic environment, we used a
237 PGW approach (Schär et al. 1996; Frei et al. 1998; Kimura and Kitoh 2007; Sato et al. 2007) as
238 has been done successfully in numerous previous studies (e.g. Mallard et al. 2013a,b; Lackmann
239 2013, 2015; Trapp and Hoogewind 2016; Gutmann et al. 2018; Jung and Lackmann 2019; Carroll-
240 Smith et al. 2020; Dougherty and Rasmussen 2020; Dougherty et al. 2023). After evaluating our
241 present-day simulations against observations (see section three), we then simulated each storm

242 with projected end-of-century conditions. To accomplish this, we calculated 20-year difference
243 fields (“deltas”) for five different temperature variables (skin temperature, surface temperature, soil
244 temperature, air temperature, and sea-surface temperature) using an ensemble of Phase 5 Coupled
245 Model Intercomparison Project (CMIP5) or CMIP6 models using the Representative Concentration
246 Pathways (RCP) 8.5 or Shared Socioeconomic Pathway (SSP) 5-8.5 emissions scenarios (Moss
247 et al. 2010; Gidden et al. 2019). These scenarios were chosen to assist the NC Department of
248 Transportation in understanding climate change flooding risks and vulnerabilities when planning
249 long-lived, resilient transportation infrastructure. We also hold relative humidity constant, which,
250 with warming, results in a moisture delta that is consistent for present-day and future environments.
251 The final step is the WRF preprocessing interpolation process that recalculates geopotential height
252 and ensures hydrostatic balance with the new virtual temperature field. For both present and
253 future simulations, we use digital filter initialization (DFI) (Lynch and Huang 1992; Peckham et al.
254 2016) to minimize high frequency noise that may occur in the model as a result of thermodynamic
255 changes, and to generate hydrometeor and cloud fields for the initial model time, reducing the need
256 for long model spin-up time.

257 For Hurricanes Matthew and Floyd, we calculated deltas using an ensemble of 20 CMIP5 models
258 for a future time period of 2080-2099 minus a historical time period of 1980-1999. This results in
259 a 100-year temperature delta, implying that our respective future storms are being represented in
260 a climate 100 years after they originally occurred. For Hurricane Florence, we instead calculated
261 deltas using an ensemble of 20 CMIP6 models for a future time period of 2080-2099 and a
262 historical time period of 1995-2014. This results in an 85-year temperature delta, implying that
263 this storm is being represented in an environment 85 years after it originally occurred. There is not
264 a distinguishable difference in the time- and ensemble-averaged projected future temperature in
265 our study region between CMIP5 and CMIP6 ensembles (not shown). The list of CMIP5 models
266 we used is the same as those used in Jung and Lackmann (2019), and the CMIP6 models we used
267 are listed in Table 2. Six of these models have equilibrium climate sensitivity (ECS) values above
268 4.5 degrees Celsius, categorizing them as “hot models” (Tokarska et al. 2020; Hausfather et al.
269 2022).

Table 2. List of CMIP6 models used to compute change fields used in Hurricane Florence PGW simulations.

<i>Models</i>		
ACCESS-CM2	ACCESS-ESM1-5	BCC-CSM2-MR
CAMS-CSM1-0	CanESM5	CESM2
CESM2-WACCM	CMCC-ESM2	CNRM-CM6-1
EC-Earth3	FGOALS-g3	GISS-E2-1-G
IPSL-CM6A-LR	MIROC6	MPI-ESM1-2-HR
MPI-ESM1-2-LR	MRI-ESM2-0	NorESM2-LM
NorESM2-MM	TaiESM1	

270 *d. Return period quantification*

271 Given larger projected changes in extreme storms in the future with additional atmospheric
 272 warming (Seneviratne et al. 2023), it is important to investigate climate change projections and
 273 the issue of non-stationary within readily available climate information especially as it relates
 274 to precipitation extremes. In particular, there is growing interest in precipitation changes and
 275 how these changes may impact hydrologic design (Wright et al. 2019; Kourtis and Tsihrintzis
 276 2022). Hydrologic design standards in North Carolina (NC) and throughout a majority of the
 277 US use existing intensity-duration-frequency (IDF) curves (NOAA Atlas 14; Bonnin et al. 2004);
 278 however, these curves do not consider non-stationarity and climate change.

279 Here we put the simulated hurricanes (now and future) in the context of NOAA Atlas 14 and a
 280 scaled version of Atlas 14 for NC (Bowden et al. 2024, 2025) that considers plausible changes using
 281 downscaled climate change projections from the Localized Constructed Analogs dataset (LOCA;
 282 Pierce et al. 2014). This method creates a regional scale factor for the eight climate divisions in
 283 NC for each General Circulation Model (GCM), different return periods, greenhouse gas emission
 284 scenarios, and time horizons of concern defined by NCDOT. An ensemble of all downscaled GCM
 285 scale factors is created and applied to scale Atlas 14. Scaling Atlas 14 is noted as a viable option
 286 (Kilgore et al. 2019) with scale factors developed for other regions using downscaled climate
 287 change projections, similar to the work presented by Miro et al. (2021) for the US Mid-Atlantic
 288 region. An assumption is made to estimate the sub-daily rainfall accumulations and intensities
 289 using the 24-hr regional scale factors. The historical and projected changes in the scaled IDF

290 values are compared with the simulated hurricanes to begin investigating non-stationarity in the
291 future IDF curves.

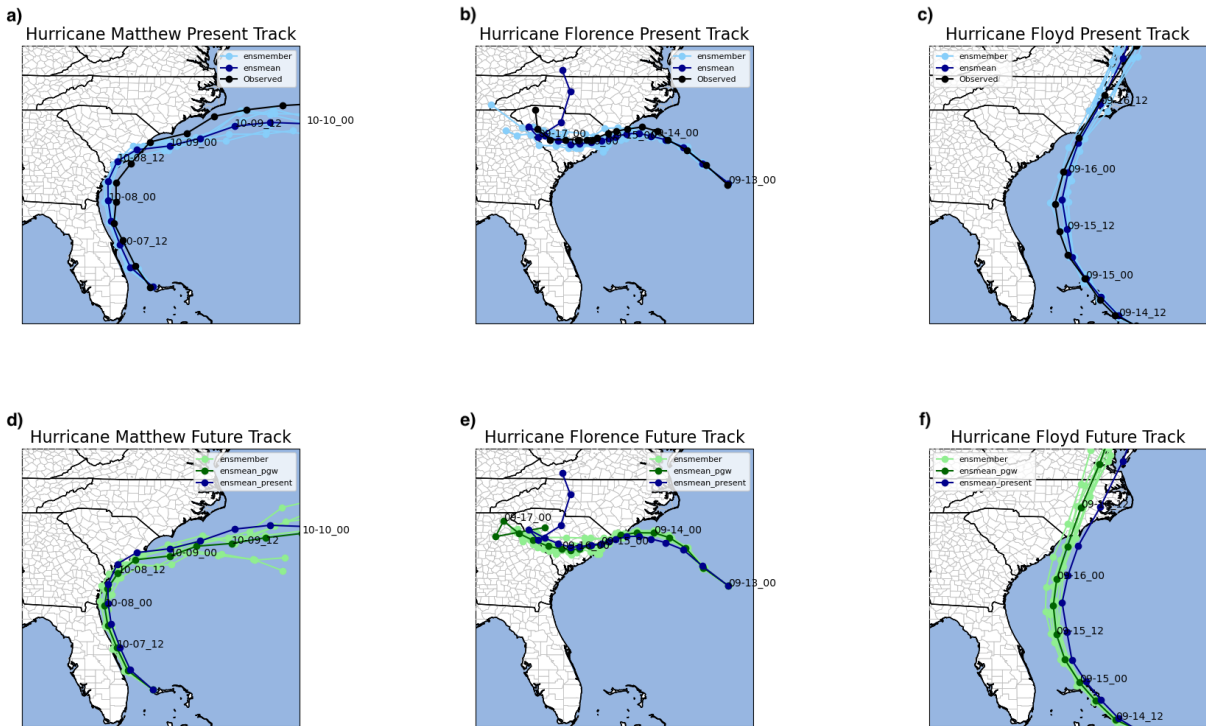
292 To calculate the return periods for our simulated storms, we store the highest 100 precipitation
293 values at nested domain grid cells for the six thresholds from each ensemble member: 1-hr, 2-hr,
294 3-hr, 6-hr, 12-hr, and 24-hr. Then, we calculate the mean and standard deviation of the stored data
295 for each time interval. For comparison, observed NOAA Atlas 14 values were selected for the
296 location in eastern North Carolina with the highest return period values, New Hanover County. We
297 chose the observed maximum IDF values in the region because the events we are simulating are
298 extreme. The future (scaled) IDF values for end-century and the same high-emission scenario for
299 the centroid county estimate are used to estimate projected rainfall for the different durations and
300 return periods.

301 **3. Model storm simulation performance**

302 *a. Present day simulations compared with observations*

303 Each ensemble mean storm track aligns fairly well with the observed tracks, with the root mean
304 square deviation (RMSD) for each storm's center falling within 130 km of the observed location.
305 Of the three storms, the ensemble mean for Floyd has the largest RMSD due to the simulated storm
306 traveling slower than observed after exiting the Carolinas. Visually, Hurricane Matthew appears
307 to exhibit the largest track error, though its RMSD is only ~75 km due to the storm deviating to
308 the west of the observed track, especially at the beginning of the simulation. We explored several
309 options to improve this issue (not shown here), however the configuration presented here represents
310 a combination of the best simulated track and precipitation distribution compared to observations.
311 The ensemble mean track for Hurricane Florence was similar to the observed, consistent with
312 smaller quantitative track errors (Table 3).

323 The intensity for the present-day simulations was more difficult to align with observations,
324 particularly for Hurricane Matthew. The large discrepancy in intensity with Hurricane Matthew
325 is expected, based on the more westward track in the simulations that resulted in greater land
326 interaction relative to observations, as well as the reanalysis representation of the intensity being
327 too weak. The RMSD of the ensemble mean central pressure for Matthew is too high by ~21-
328 hPa (Table 3). While this is a large difference, the precipitation values over North and South



313 Figure 5. Storm tracks of Hurricanes Matthew (a,d), Florence (b,e), and Floyd's (c,f) ensemble members,
 314 ensemble mean, and observed NHC storm for the present-day simulations (a-c) and future simulations (d-f). The
 315 black line represents the NHC best track locations, the lighter blue (green) represents the ensemble members,
 316 and the darker blue (green) represents the ensemble mean for the present (future) storms.

329 Carolina still compared well with observations (Fig. 2a,d). Given that the precipitation from
 330 Hurricane Matthew was influenced by extratropical interaction, we accepted the intensity error in
 331 these simulations. Simulated intensities for Hurricanes Floyd and Florence aligned much better
 332 with observations, with error values of only ~ 5 and ~ 7 -hPa, respectively (Table 3).

333 As mentioned above, an additional metric we used to ensure the validity of our runs was the
 334 similarity between the observed and modeled total accumulated precipitation for each storm (Fig.
 335 2a-f). We subjectively analyzed each storm's simulated ensemble probability matched mean
 336 accumulated precipitation and compared its spatial footprint and maximum precipitation amounts
 337 with the Stage IV precipitation for Hurricanes Matthew and Florence, and Livneh precipitation for
 338 Hurricane Floyd. Overall, the spatial footprint of the accumulated precipitation aligns well for all
 339 of our storms, but the maximum storm total precipitation differs largely for Hurricanes Matthew

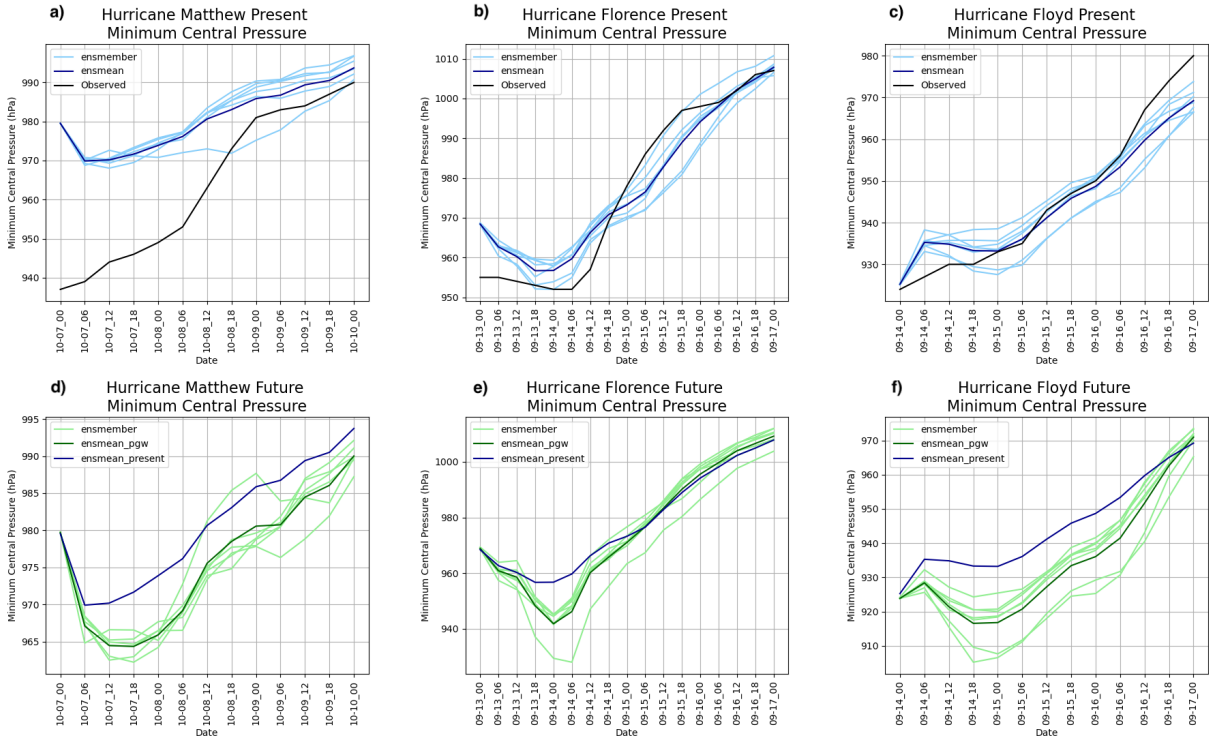


Figure 6. As in Fig. 5 but with minimum central pressure for each storm (hPa).

340 and Floyd. Considering the track, intensity, and precipitation similarities, we deemed the ensemble
 341 simulations sufficient to proceed with analysis.

342 *b. Present day compared with future simulations*

343 Comparing the resulting present-day and future ensemble mean storm tracks, we find that, as
 344 expected, they are quite similar for all storms (Fig. 5). While subtle track differences do exist
 345 with each storm, overall their tracks are sufficiently similar to allow for precipitation comparisons,
 346 especially given that many of the comparisons will be done via an averaging box over North and
 347 South Carolina land points (Fig. 4). For each of our storms, the future ensemble mean track falls
 348 within a reasonable distance from the present ensemble mean, with the RMSD track difference for
 349 Matthew and Florence being less than 40 km, and for Floyd less than 60 km (Table 3).

350 The future simulations for all storms also reach lower ensemble mean minimum central pressures
 351 than their respective present-day counterparts (Fig. 6). The largest intensity difference occurs with
 352 Hurricane Floyd, which, at its highest intensity, features a minimum central pressure that is 17-hPa
 353 lower in the future ensemble mean relative to the reanalysis simulations of Floyd. Comparing

317 Table 3. Track and intensity comparison summary. Great-circle distances RMSD (km) are shown in column
 318 one, while the storm minimum sea-level pressure RMSD (hPa) are shown in column two. Rows one through
 319 three are comparing observed values (NHC best track) with simulated present ensemble mean values (simulated
 320 minus observed), and rows four through six are comparing present ensemble mean values with future ensemble
 321 mean values for each storm (present minus future). Differences are calculated every six hours then averaged
 322 across all model times (13 times for Floyd and Matthew, 16 for Florence).

	<i>Avg track RMSD (km)</i>	<i>Avg minimum central pressure RMSD (hPa)</i>
Matthew Present to Observations	75.7	21.1
Florence Present to Observations	29.3	6.8
Floyd Present to Observations	126.3	4.9
Matthew Present to Future	38.6	5.4
Florence Present to Future	37.1	5.9
Floyd Present to Future	59.6	11.6

354 that with the average difference between the present and future ensemble mean minimum central
 355 pressure, the largest difference between the present and future also exists for Hurricane Floyd,
 356 which has a 12-hPa difference (Table 3).

357 **4. Changes in precipitation characteristics**

358 *a. Total accumulated precipitation*

359 Several TC rainfall metrics can be used to quantify the complete nature of TC precipitation
 360 change with climate change. One such metric is the total amount of precipitation that a system
 361 produces over land, for example, total accumulated rainfall at all land grid cells (Fig. 2). In the
 362 PGW simulations, the tracks deviate slightly, resulting in an associated shift of the precipitation
 363 swath which can complicate using a direct grid-cell difference between the present and future

378 Table 4. Change in the whole-domain land area receiving rainfall thresholds of greater than 10 in (250 mm),
 379 15 in (375 mm), 20 in (500 mm), and 30 in (750 mm). Also shown are the average percent change in total area
 380 receiving rainfall for regions only over land as well as over the land and ocean.

	<i>Matthew</i> (2016)	<i>Florence</i> (2018)	<i>Floyd</i> (1999)
250 mm.	$17600 \pm 800km^2$	$9800 \pm 500km^2$	$22400 \pm 400km^2$
375 mm.	$27000 \pm 500km^2$	$9900 \pm 400km^2$	$9900 \pm 300km^2$
500 mm.	$14000 \pm 100km^2$	$9000 \pm 500km^2$	$1300 \pm 100km^2$
750 mm.	$2200 \pm 100km^2$	$4600 \pm 300km^2$	—
average change over our study region (land only)	+14%	+36%	+110%
average change over our study region (including ocean)	+68%	+40%	+130%

364 accumulated precipitation. However, we can still visually see an expansion of the 375-mm isohyet
 365 (~15 in) in all three cases (Fig. 2). Examining a variety of thresholds, we see an increase in the
 366 area receiving greater than 250, 375, 500, and 750 mm of accumulated rainfall in all future cases
 367 where those thresholds are met (Table 4). The largest areal increase for Floyd occurred where
 368 precipitation totals exceeded 250 mm ($22400 \pm 400km^2$), for Matthew where precipitation totals
 369 exceeded 375 mm ($27000 \pm 500km^2$), and for Florence where precipitation totals exceeded 375 mm
 370 ($9900 \pm 400km^2$). Amongst the three storms, we see the largest areal increase in precipitation for
 371 any threshold above 250 mm in Hurricane Matthew ($27000 \pm 500km^2$ for areas receiving greater
 372 than 375 mm). Hurricane Florence’s largest areal increase for any threshold is less than Matthew
 373 and Floyd’s largest changes by about half, indicating it had the smallest changes in footprint for
 374 high accumulated precipitation amounts (Table 4). Looking at just the change in the maximum
 375 accumulated precipitation value for a single grid cell over the Carolinas, we also see an increase
 376 for all storms, though the range is quite large between the three storms (+7% for Floyd, +90% for
 377 Matthew, and +46% for Florence) (not shown).

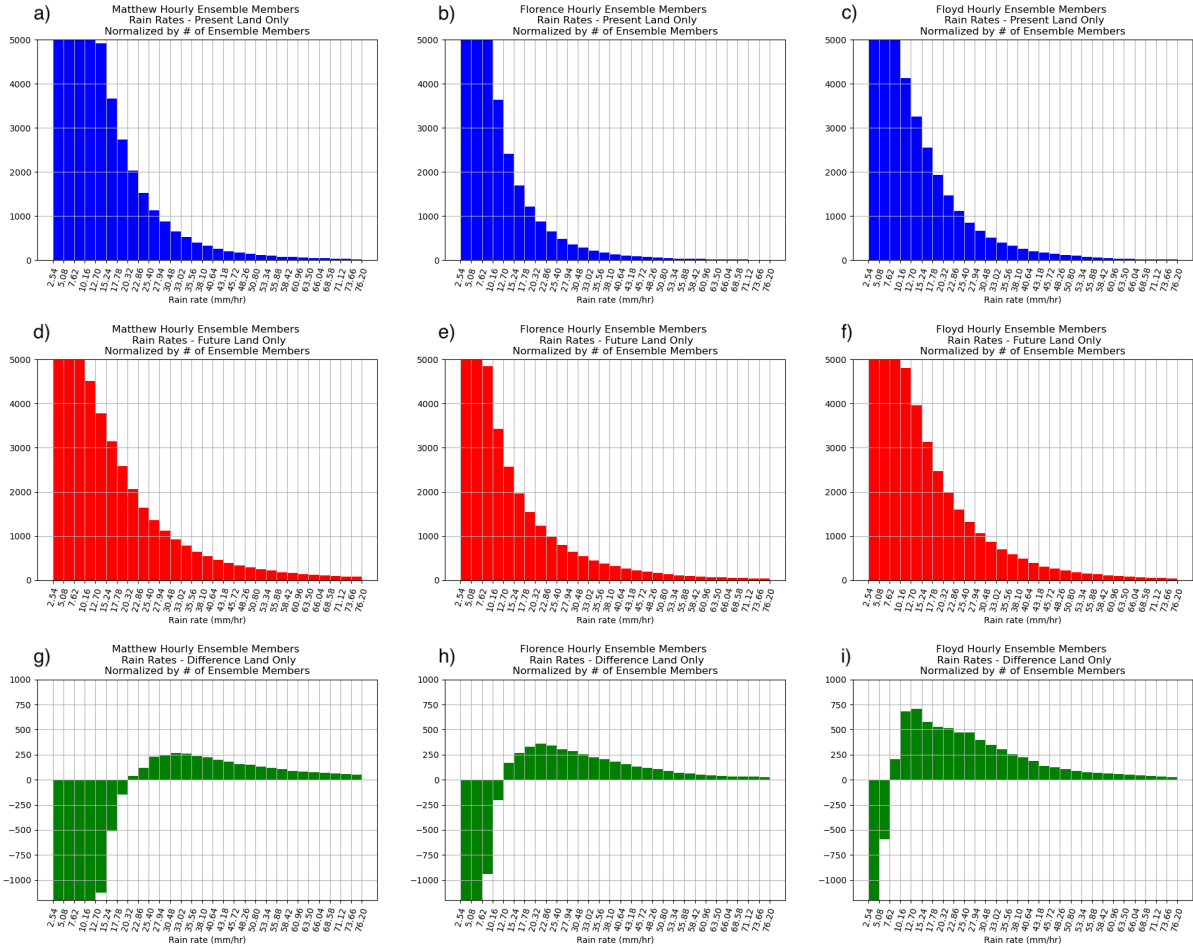
381 Most studies that evaluate TC rain rates and climate change report their percent changes as an
 382 average over a large area, making it difficult to compare when considering a much smaller region.

383 However, Wright et al. (2015) found that for North and South Carolina, when comparing rainfall for
384 present time-period TCs with future projections from CMIP3, early CMIP5, and late CMIP5, the
385 spatial map of percent changes in rainfall show increased values ranging from 50 to 150% across
386 our study region. This is quite similar to what we find here with over 100% increases in rainfall
387 for all three storms in parts of North and South Carolina (not shown here). It is important to note,
388 however, that in our study we use RCP8.5 and Wright et al. (2015) used RCP4.5/A1B. Liu et al.
389 (2018) also evaluated how eastern US landfalling TC rainfall would evolve with climate change, and
390 in doing so found that for landfalling TCs between July and November, the increase in rainfall over
391 North and South Carolina ranged from 0-40% for the RCP4.5 future scenario. The precipitation
392 increases for our storms varies widely across our study region, with maximum increases as high
393 as 150% in some places. The large differences between their study and ours may be due in part to
394 their model resolution being much coarser than ours (50-km grid spacing compared to 4-km). Ours
395 are also three specific, extreme cases as compared to years-long composites of multiple storms.

396 *b. Distribution of rain rates*

397 An important precipitation characteristic is the distribution of over-land rain rates for each of the
398 storms, and how those distributions change in a warmer climate (Fig. 7). All three storms exhibit
399 a decrease in the frequency of weaker rain rates (less than 12 mm per hour) and an increase in rain
400 rates greater than 25 mm per hour, with Florence and Floyd showing future increases at all rain
401 rates above 12 mm per hour. The biggest future increase in the occurrence of a given rain rate
402 varies by storm, with Matthew having the largest increase around 30 to 33 mm (1.2 to 1.3 inches)
403 per hour, Florence having the largest increase around 20 to 23 mm (0.8 to 0.9 inches) per hour,
404 and Floyd having the largest increase around the 12 to 15 mm (0.5 to 0.6 inches) per hour range,
405 when only considering rain rates above 12 mm per hour. The overall pattern of a decrease in the
406 frequency of lower rain rates and increase in the frequency of higher rain rates aligns with previous
407 studies (Lackmann 2013; Gutmann et al. 2018), and also points to the potential for our future
408 storms to have higher flash-flooding potential than their present-day counterparts. A subsequent
409 paper will explore the causes for this change in rain rate distribution.

416 As mentioned previously, a central finding of studies that examine changes in TC precipitation
417 is an increase in rainfall that either follows or exceeds the Clausius-Clapeyron (CC) scaling ($\sim 7\%$



410 Figure 7. Histograms of ensemble mean rain rate (mmh^{-1}) for Hurricanes Matthew (a,d,g), Florence (b,e,h),
 411 and Floyd (c,f,i). Here we plot rain rates from present-day WRF ensemble members (a-c), future WRF ensemble
 412 members (d-f), and the difference between the two (g-i). The counts are number of cells that experienced that rain
 413 rate in any ensemble members, normalized by the number of ensemble members. These are also only showing
 414 rain rates that occur over land points in our region of interest. Values greater than 5000 are omitted to allow
 415 focus on the higher rain rate values.

418 increase per degree Celsius of warming) (Knutson and Tuleya 2004; Hill and Lackmann 2011;
 419 Knutson et al. 2015). For all of our simulations, the average temperature increase across the
 420 lower and middle atmosphere (surface to 500 hPa) from present to future was $\sim 4.5\text{K}$ (Table 5).
 421 This temperature increase implies a vapor increase of $\sim 35\%$ for all storms. When we calculate the
 422 percentage change in precipitable water (PWAT), we find that all three storms have PWAT increases
 423 just under the expected vapor increase given by the CC scaling - these variations are understandable

432 Table 5. Temporally and spatially averaged changes in atmospheric layer temperature (surface-500 hPa) and
 433 precipitable water calculated from the present-day ensemble mean files. Mean hourly rain rates and standard
 434 deviations are calculated from all of the ensemble members for each storm. The percent changes are calculated
 435 from the ensemble member means and ensemble member 90th percentile precipitation calculations. The plus or
 436 minus error metrics represent one standard deviation.

	<i>Matthew</i> (2016)	<i>Florence</i> (2018)	<i>Floyd</i> (1999)
Temperature change	+4.5K	+4.5K	+4.5K
Expected CC scaling	35%	36%	36%
Present PWAT	40.9 mm	45.3 mm	43.6 mm
Future PWAT	54.2 mm	58.1 mm	57.4 mm
PWAT percent change	32%	28%	31%
Present mean rain rate	$11.6 \pm 0.4 \text{ mmh}^{-1}$	$9.2 \pm 0.7 \text{ mmh}^{-1}$	$12.1 \pm 0.8 \text{ mmh}^{-1}$
Future mean rain rate	$14.3 \pm 1.2 \text{ mmh}^{-1}$	$12.3 \pm 0.7 \text{ mmh}^{-1}$	$14.6 \pm 1.1 \text{ mmh}^{-1}$
Mean rain rate %	$23 \pm 9\%$	$34 \pm 12\%$	$21 \pm 6\%$
90th percentile rain rate %	$37 \pm 7\%$	$55 \pm 20\%$	$25 \pm 8\%$

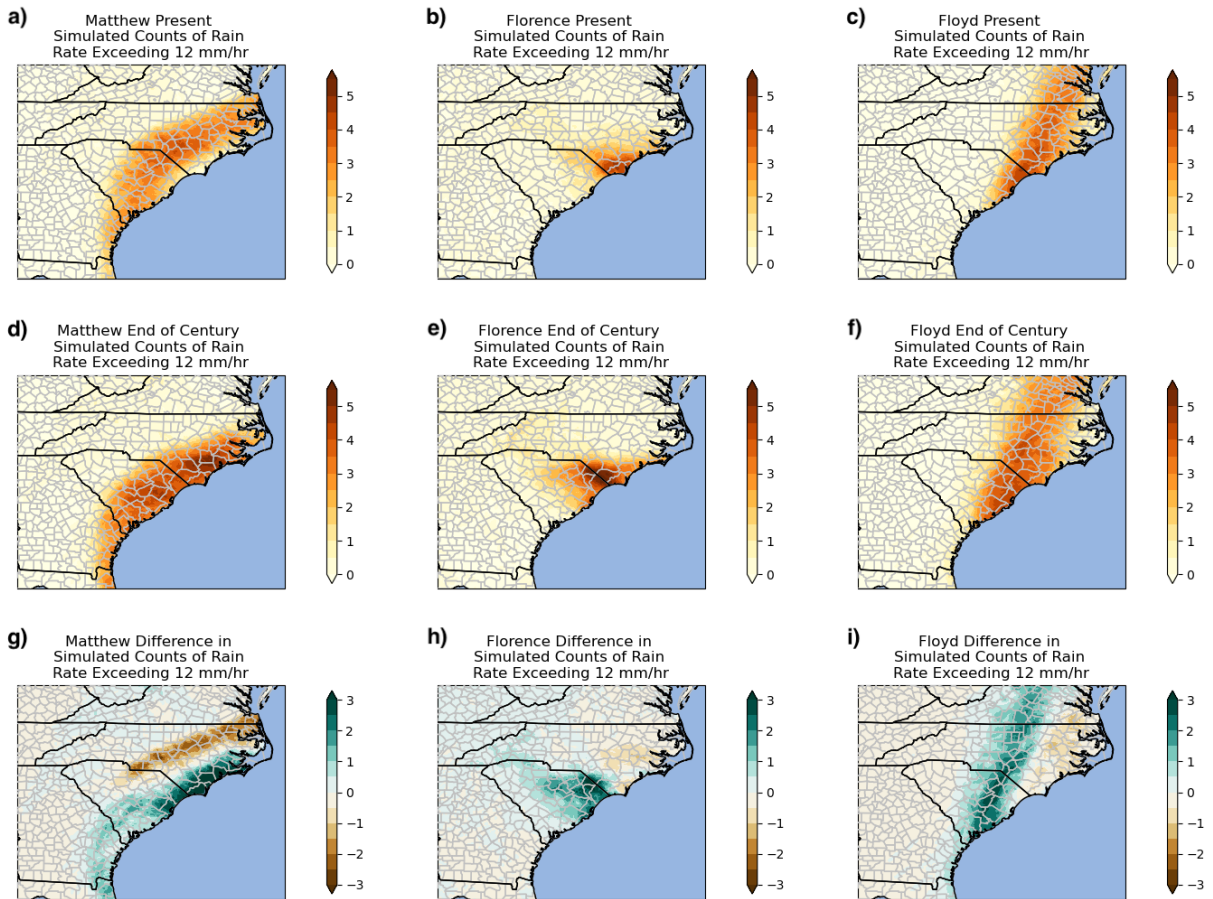
424 given that we averaged the 4.5K temperature change across height and location. Comparing the
 425 average rain rates from the histograms, we find percent increases of $23 \pm 9\%$, $34 \pm 12\%$, and $21 \pm 6\%$
 426 for Hurricanes Matthew, Florence, and Floyd respectively (Table 5), which are sub-CC scale, CC
 427 scale, and sub-CC scale, respectively. When we consider the changes in the 90th percentile of
 428 these distributions, or the more extreme rain rates, we find increases of $37 \pm 7\%$, $55 \pm 20\%$, and
 429 $25 \pm 8\%$ for Hurricanes Matthew, Florence, and Floyd respectively (Table 5), which are CC scale,
 430 super-CC scale, and sub-CC scale respectively. For all three storms, this implies that the extreme
 431 precipitation rates are increasing more than the averages.

437 *c. Areal extent of rain rates*

438 While the frequency of rain rate occurrences is valuable, it is also important to see where
439 these rain rates occur to determine if the spatial extent of heavy rain rates changes along with
440 the distribution. These plots are also useful to show us regions that may have experienced these
441 rain rates multiple times, thus exacerbating impacts (Fig. 8). The heat map for greater than 12.7
442 mmh^{-1} of rain is presented here, but larger thresholds were also computed (not shown). The largest
443 difference these heat maps reveals is a shift in track between the present ensemble members and
444 the future ensemble members for all storms. Along with the track shift, however, we also see an
445 expansion of the regions experiencing greater than 12.7 mmh^{-1} rain rates (Fig. 8). When we
446 average the amount of grid cells in which the frequency of rain rates exceeds 12.7 mmh^{-1} , we
447 find increases of 20%, 28%, and 28% for Hurricanes Matthew, Florence, and Floyd respectively.
448 When we average the highest 5% of these frequency values, which gives an idea of how much
449 the area of repeated rain rate occurrence changes, the percent increases are 17%, 47%, and 21%
450 for Hurricanes Matthew, Florence, and Floyd respectively. These precipitation quantities can be
451 useful to planners and state agencies as it gives insight into another potential cause of flooding or
452 flash-flooding: duration of high-intensity rain rates.

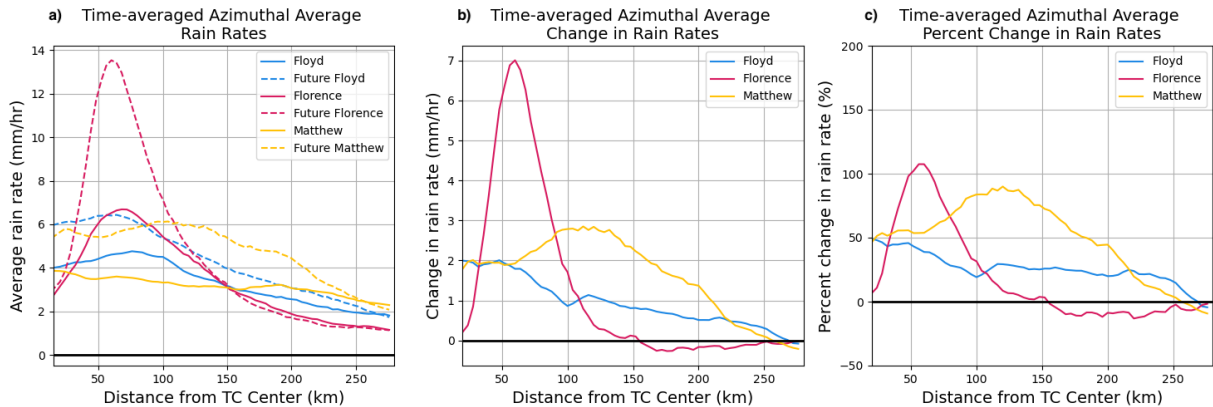
456 *d. Storm-Centered Precipitation Changes*

457 Because of present to future track shifts, it is useful to consider storm-centered precipitation
458 changes by considering the distance from the TC center where the highest rain rates are occurring,
459 and how that may shift with climate warming. As has been shown in previous TC and ET literature
460 (Atallah et al. 2007; Liu et al. 2018; Jung and Lackmann 2019, 2021), TCs with more tropical
461 characteristics see the highest rain rate increases near the TC center; then, as the storm begins to
462 undergo ET, the region of maximum rain rates extends outward away from the TC center. Since
463 our storms are in various stages of ET when they impact North Carolina, we evaluate where the
464 maximum rain rates exist in relation to the distance from the TC center, and how that changes with
465 warming. To do this, we calculated the azimuthal average rain rate values for all of our storms
466 across all simulation times (not shown) and then averaged across the simulation time (Fig. 9). For
467 the storm that most strongly retained tropical characteristics, Florence, we find that in the future
468 the largest rain rate increase of $\sim 110\%$ occurs between 50 and 100 km from the storm center. For



453 Figure 8. As in Fig. 7 but showing instances of rain rates greater than 12.7 mmh^{-1} occurring in each grid cell
 454 normalized by the number of ensemble members and the number of days in the simulation to allow for a better
 455 comparison between storms.

469 Matthew, which was closest to transition while it was impacting the Carolinas, we see the largest
 470 increase in rain rates further from the TC center between 100 and 150 km. The mean magnitude of
 471 this difference is an increase of $\sim 90\%$ from present to future. Floyd, which exhibited both tropical
 472 and extratropical characteristics when its rain bands were over South and North Carolina, exhibits
 473 a double peak: the first within 50 km and the second between 100 and 150 km. The magnitudes
 474 of these increases peak at about 50% and 30%, respectively. Both the highest simulated mean rain
 475 rates and the largest percent increases in rain rates from present to future were associated with
 476 Hurricane Florence.



485 Figure 9. Time mean azimuthal average rain rates for Hurricanes Matthew, Florence, and Floyd for the present
 486 and future ensemble mean (a); difference between each storm's present and future (b); and percent change in
 487 rain rates (c). These values are for rain rates that occurred over the land and ocean in the averaging area over the
 488 Carolinas shown in Fig. 4.

477 The values shown here are for rain rates that occurred over ocean and land in our Carolinas
 478 averaging box; if we instead consider the whole domain 4-km that our storms moved through (not
 479 shown), we find that all storms have a rain rate peak within 100 km of the center (as Florence does
 480 in Fig. 9) and Matthew and Floyd exhibit a second rain rate peak between 100 and 200 km. The
 481 largest rain rates and the largest increase in rain rates are in future Hurricane Floyd within 75 km of
 482 the storm center. While this provides context to the tropical and extratropical-transitioning nature
 483 of the full life cycle of these storms, our area of primary interest is the Carolinas, where Florence
 484 was tropical and Floyd and Matthew were being influenced by baroclinic systems.

489 *e. Changes in return period of precipitation*

490 The return period can be used to quantify extreme precipitation events in the context of historical
 491 events. Here, we quantify the return period for all three storms for different precipitation time
 492 intervals (1-hr, 2-hr, 3-hr, 6-hr, 12-hr, and 24-hr; Fig. 10). For all cases, the future storms
 493 had a higher return period (e.g., from 100-yr to 500-yr) than the present-day version for all time
 494 intervals. At the shorter time intervals, Hurricanes Matthew and Florence exhibit the largest
 495 increases in maximum rain rate, with future Matthew exhibiting larger values than Florence at all
 496 times shown. When we consider the longer time intervals (i.e. 12-hr and 24-hr), we find that

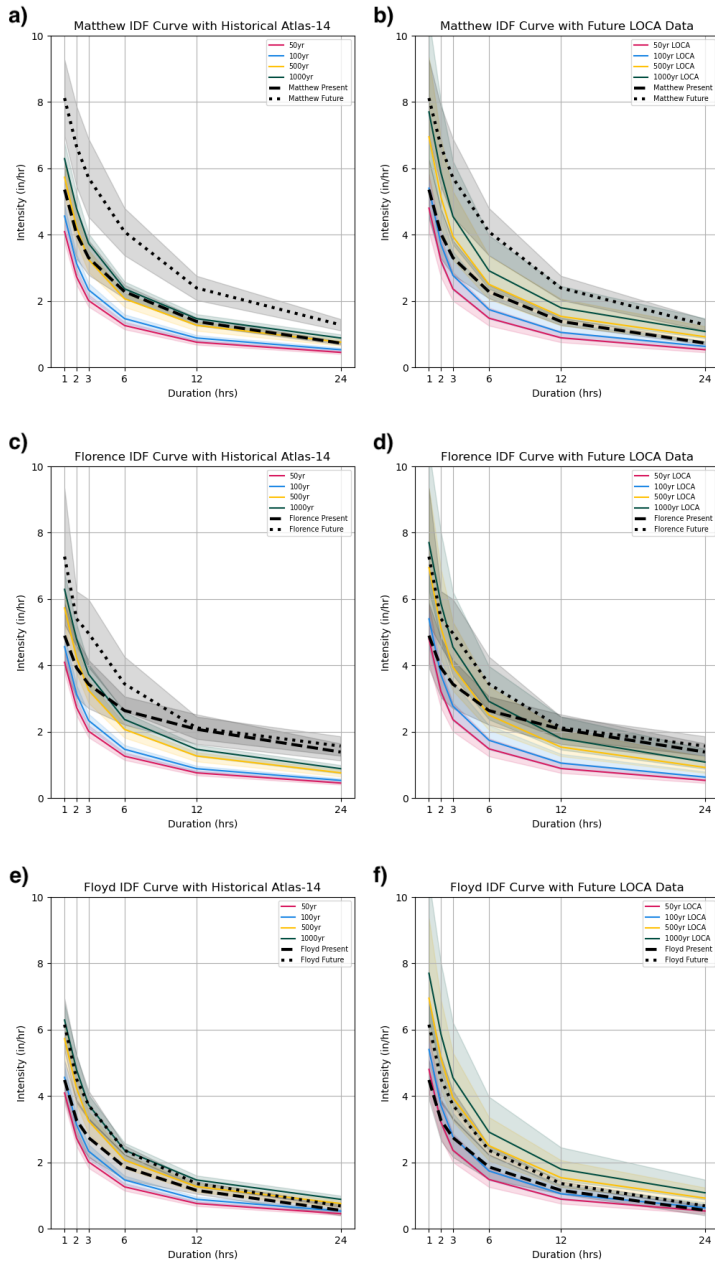
497 Hurricane Florence has larger increases - this is not surprising as Hurricane Florence was a much
498 longer duration storm than either Matthew or Floyd.

505 When we consider all of these precipitation values in the context of the climate-model (LOCA)
506 adjusted Atlas-14 data, all storms in the present and future and at each rainfall duration period shift
507 to lower return intervals (i.e. if we consider 50, 100, 500, and 1000 year return periods, they shift
508 from 500 to 50 or 1000 to 100 when comparing with historical versus LOCA). Even with these
509 adjustments, however, future Florence and future Matthew are still greater than 1000 year events for
510 all six time intervals we consider here. This speaks to just how rare these storms were historically,
511 and how in a future scenario they can become more frequent but still have even more extreme
512 precipitation. However, this also may suggest that LOCA fails to represent TC precipitation, and
513 that what appears here to be a 1000-year event may not be quite as rare.

514 **5. Conclusions**

515 Tropical cyclone rain rates are expected to increase as the climate continues to warm, but the extent
516 of that increase and how it may differ for TCs at different stages in their life cycle, or in contrasting
517 synoptic environments, is less clear. Here, by evaluating over-land rain rate characteristics of
518 three Atlantic TCs at various stages of their life cycles, in diverse synoptic patterns, and in altered
519 climate conditions, we find that there is strong variability amongst the three storms for multiple
520 rainfall characteristics: accumulated rain, distribution of rain rates, spatial distribution of rain
521 rates, and historical extremity of rain rates. We evaluated these three synoptically diverse TC
522 events using high-resolution ensembles in the current climate, and for a high-emission end-of-
523 century thermodynamic environment (RCP 8.5 and SSP585). The main results for changes in each
524 precipitation characteristic are as follows:

- 525 • For storm-total accumulated rainfall, the area receiving at least 250mm of rainfall expanded
526 by $17600 \pm 800km^2$, $9800 \pm 500km^2$, and $22400 \pm 400km^2$ for Hurricanes Matthew, Florence,
527 and Floyd, respectively - Hurricanes Matthew and Floyd had almost double the areal expansion
528 as Florence did. The largest areal expansions for each storm occurred at greater than 375 mm
529 for Matthew, greater than 375 mm for Florence, and greater than 250 mm for Floyd.
- 530 • When considering how the rain rates changed for each storm, we see an increase in all rain rates
531 greater than 5 mmh^{-1} for each storm, and a decrease in the rain rates below that threshold.



499 Figure 10. Intensity Duration Frequency curves for historical Atlas-14 values for the New Hanover County
 500 station in eastern North Carolina (a, c, e) and for the updated, end-of-century values which include the climate
 501 signal from LOCA statistically downscaled climate data (b, d, f). The curves shown represent the 50, 100, 500,
 502 and 1000 year return period values for 1, 2, 3, 6, 12, and 24 hour time periods. They represent the average and
 503 standard deviation for the 100 highest rain rate values for Hurricanes Matthew (a, b), Florence (c, d), and Floyd
 504 (e, f) from the present simulations (dashed line) and future simulations (dotted line).

532 We also find that, while Matthew and Floyd have higher average rain rates in the present
533 and future, Florence has the highest percent increase in both the average rain rates and 90th
534 percentile rain rates ($34 \pm 12\%$ and $55 \pm 20\%$).

- 535 • Each storm exhibits a greater than 19% increase in rain rates greater than 12.7 mmh^{-1} , and
536 a greater than 17% increase in the number of hours during which those rain rates occurred.
537 The largest increases in both of these metrics exist with Hurricane Florence (28% and 47%
538 respectively).
- 539 • The most discernible differences between these storms emerge when we consider time-
540 averaged rain rates as a function of distance from the TC center. For Hurricane Florence, a
541 storm that strongly retained tropical characteristics, the highest values and the largest change
542 in rain rate occur within 100 km of the center. Matthew and Floyd, both transitioning storms
543 interacting with synoptic features, exhibited peak rain rates further from the TC center at
544 distances greater than 100 km. Both the highest rain rate of any storm and the largest increase
545 in mean rain rate occurred with Hurricane Florence.
- 546 • Each of our future storms was greater than a 100-year event for multiple rainfall periods
547 when considering both the historical Atlas-14 scale as well the LOCA-adjusted Atlas-14 that
548 accounts for climate change. Hurricane Matthew's 1-hr, 2-hr, 3-hr, and 6-hr future maximum
549 rain rates were the highest out of all three storms, while Florence had the highest future
550 maximum rain rates for 12-hr and 24-hr duration.

551 The ensemble of present-day and future simulations can be used to assess future threats, for
552 example to transportation infrastructure. For such applications, where highly localized present-to-
553 future comparisons are needed, a “scale factor” approach is useful because it eliminates challenges
554 created by the shifts in the spatial precipitation distribution. For such applications, we recommend
555 computing precipitation change statistics from the present-day and future ensembles to determine
556 scale factors, such as the percent changes we calculated from the histograms here. Then, the
557 scale factor can be applied to either observed or simulated present-day precipitation. For more on
558 this approach, see Grimley et al. (2024). This scale-factor approach can be modified to consider
559 different storm types, different percentile thresholds, or different regions.

560 The configuration of this study has a few limitations, one of which is the use of spectral nudging.
561 Two of these storm simulations utilized nudging to encourage the storms to follow similar tracks in
562 the present and the future. We acknowledge that the nudged track is not the track these storms likely
563 would have taken in a future climate without nudging, and therefore these simulations should not be
564 used to add to the conversation about shifts in future storm tracks. This nudging could have resulted
565 in minor environmental influences that may have impacted the resulting precipitation fields, though
566 only the large-scale steering flow was nudged in an attempt to minimize this influence.

567 Another limitation of this study is the limited sample size of storms studied; only three storms
568 are compared, all of which are relatively weak intensities and only represent a subset of synoptic
569 environments. We also are only examining one future scenario (RCP8.5) out of many, and one
570 future time period out of many (end of century). While we acknowledge that three storms in one
571 future scenario is not sufficient to fully generalize future TC rainfall changes for storms in a large
572 variety of synoptic settings, and a larger catalog of storms would be preferred in order to represent
573 the variability, there are still some patterns we can identify from our subset of storms. One such
574 pattern is that, while Hurricanes Floyd and Matthew have larger average rain rates in the present
575 and future than Florence (when considering the whole distribution of rain rates), we find the largest
576 percent increases in average rain rate with Hurricane Florence. When we consider these rain rate
577 changes as a function of distance from the TC center, we see that again the largest percent increases
578 in average rain rates exist with Hurricane Florence within 100-km of the storm center. However,
579 Hurricane Florence also has a much smaller areal increase in total accumulated precipitation than
580 both Matthew and Floyd when we consider totals above 250mm. These findings may point to
581 a difference in climate change response for more tropical, non-synoptic TC rainfall as compared
582 to more extratropical-transitioning, synoptic-interacting TCs. In a subsequent paper, the forcing
583 mechanisms for these precipitation changes will be evaluated to understand what thermodynamic
584 and dynamic mechanisms are contributing to these discrepancies in TC precipitation changes by
585 synoptic environment.

586 Each of these storms produced substantial rainfall when they occurred historically, and the
587 changes described above indicate that if similar storms occurred in a future, warmer climate, the
588 impacts could be even more devastating. We also highlight the importance of evaluating these
589 precipitation changes as a function of the environment the TC is in. It is important to understand

590 how TC rainfall, evaluated from multiple different lenses at different spatial scales, may change as
591 the climate continues to warm in order to help inform infrastructure planning, as well as to assist
592 in attempts to mitigate damage and loss of life caused in the wake of these destructive TCs.

593 *Acknowledgments.* This research was supported by the North Carolina Department of Transporta-
594 tion project 2020-57, awarded to North Carolina State University (NCSU), and North Carolina State
595 Hydraulics Engineer, Matthew Lauffer. High-performance computing support was provided by
596 the North Carolina State University Henry2 and Hazel clusters. Thanks to Chunyong Jung for
597 obtaining and interpolating the CMIP5 GCM data and providing the interpolation codes, and to
598 Brett Roberts for code and assistance with calculating probability matched mean precipitation. We
599 also thank Lauren Grimley and Lauren Getker for feedback on an earlier version of the manuscript.

600 *Data availability statement.* The source code for the model used in this study,
601 WRF 4.2.2, is freely available from [https://github.com/wrf-model/WRF/releases?](https://github.com/wrf-model/WRF/releases?page=2)
602 [page=2](https://github.com/wrf-model/WRF/releases?page=2). Model output from the simulations presented in this manuscript are
603 available at <https://doi.org/10.5061/dryad.x95x69pt8>. ECMWF 5 reanaly-
604 sis data can be obtained from [https://cds.climate.copernicus.eu/cdsapp#!/](https://cds.climate.copernicus.eu/cdsapp#!/dataset/reanalysis-era5-pressure-levels?tab=form)
605 [dataset/reanalysis-era5-pressure-levels?tab=form](https://cds.climate.copernicus.eu/cdsapp#!/dataset/reanalysis-era5-pressure-levels?tab=form), CFSR data can be ob-
606 tained from [https://www.ncei.noaa.gov/data/climate-forecast-system/access/](https://www.ncei.noaa.gov/data/climate-forecast-system/access/reanalysis/6-hourly-by-pressure-level/)
607 [reanalysis/6-hourly-by-pressure-level/](https://www.ncei.noaa.gov/data/climate-forecast-system/access/reanalysis/6-hourly-by-pressure-level/), and GDAS/FNL data can be obtained from
608 <https://rda.ucar.edu/datasets/ds083.3/dataaccess/#>.

609 **References**

- 610 Atallah, E., L. F. Bosart, and A. R. Aiyyer, 2007: Precipitation distribution associated with
611 landfalling tropical cyclones over the eastern united states. *Mon. Wea. Rev.*, **135**, 2185–2206,
612 <https://doi.org/10.1175/MWR3382.1>.
- 613 Atallah, E. H., and L. F. Bosart, 2003: The extratropical transition and precipitation distribution
614 of hurricane floyd (1999). *Mon. Wea. Rev.*
- 615 Baulenas, E., G. Versteeg, M. Terrado, J. Mindlin, and D. Bojovic, 2023: Assembling the climate
616 story: use of storyline approaches in climate-related science. *Global Challenges*, 2200183.
- 617 Bieli, M., A. H. Sobel, S. J. Camargo, H. Murakami, and G. A. Vecchi, 2020: Application of the
618 cyclone phase space to extratropical transition in a global climate model. *Journal of Advances
619 in Modeling Earth Systems*, **12** (4), e2019MS001878, [https://doi.org/https://doi.org/10.1029/
620 2019MS001878](https://doi.org/https://doi.org/10.1029/2019MS001878).
- 621 Bonnin, G. M., D. Martin, B. Lin, T. Parzybok, M. Yekta, and D. Riley, 2004: Precipitation-
622 frequency atlas of the united states. volume 2 version 3.0. delaware, district of columbia, illinois,
623 indiana, kentucky, maryland, new jersey, north carolina, ohio, pennsylvania, south carolina,
624 tennessee, virginia, west virginia. Tech. rep., U.S. Department of Commerce.
- 625 Bowden, J. H., K. E. Kunkel, G. M. Lackmann, K. Hollinger Beatty, K. Dello, A. M. Jalowska, T. L.
626 Spero, and M. Lauffer, 2025: An apples-to-apples comparison of downscaling methods to inform
627 and produce future precipitation intensity-duration-frequency curves for resilient transportation
628 within north carolina, in preparation.
- 629 Bowden, J. H., T. L. Otte, C. G. Nolte, and M. J. Otte, 2012: Examining interior grid nudging
630 techniques using two-way nesting in the wrf model for regional climate modeling. *Journal of
631 Climate*, **25** (8), 2805–2823.
- 632 Bowden, J. H., and Coauthors, 2024: A comparison of downscaling methods to create future pre-
633 cipitation intensity-duration-frequency curves for resilient transportation within north carolina.
634 *104th AMS Annual Meeting*, AMS.

- 635 Carroll-Smith, D., R. J. Trapp, and J. M. Done, 2020: Exploring inland tropical cyclone rainfall
636 and tornadoes under future climate conditions through a case study of hurricane ivan. *J. Appl.*
637 *Meteor. Climatol.*, **60**, 103–118, <https://doi.org/10.1175/JAMC-D-20-0090.1>.
- 638 Colle, B. A., 2003: Numerical simulations of the extratropical transition of floyd (1999): Structural
639 evolution and responsible mechanisms for the heavy rainfall over the northeast united states. *Mon.*
640 *Wea. Rev.*
- 641 Donelan, M., B. K. Haus, N. Reul, W. Plant, M. Stiassnie, H. Graber, O. B. Brown, and E. Saltzman,
642 2004: On the limiting aerodynamic roughness of the ocean in very strong winds. *Geophysical*
643 *Research Letters*, **31** (18).
- 644 Dougherty, E., and K. L. Rasmussen, 2020: Changes in future flash flood–producing storms in the
645 united states. *J. Hydrometeor.*, **21**, 2221–2236, <https://doi.org/10.1175/JHM-D-20-0014.1>.
- 646 Dougherty, E. M., A. F. Prein, E. D. Gutmann, and A. J. Newman, 2023: Future simulated
647 changes in central u.s. mesoscale convective system rainfall caused by changes in convective
648 and stratiform structure. *Journal of Geophysical Research: Atmospheres*, **128**, <https://doi.org/10.1029/2022JD037537>.
- 650 Evans, C., and Coauthors, 2017: The extratropical transition of tropical cyclones. part i:
651 Cyclone evolution and direct impacts. *Mon. Wea. Rev.*, **145**, 4317–4344, <https://doi.org/10.1175/mwr-d-17-0027.1>.
- 653 Frei, C., C. Schär, D. Lüthi, and H. C. Davies, 1998: Heavy precipitation processes in a warmer
654 climate. *Geophys. Res. Lett.*, **25**, 1431–1434, <https://doi.org/10.1029/98GL51099>.
- 655 Gidden, M. J., and Coauthors, 2019: Global emissions pathways under different socioeconomic
656 scenarios for use in cmip6: a dataset of harmonized emissions trajectories through the end
657 of the century. *Geoscientific Model Development*, **12** (4), 1443–1475, <https://doi.org/10.5194/gmd-12-1443-2019>.
- 659 Grimley, L. G., K. E. Hollinger Beatty, A. Sebastian, S. Bunya, and G. M. Lackmann, 2024:
660 Climate change exacerbates flooding from recent tropical cyclones, in preparation.

661 Gutmann, E. D., and Coauthors, 2018: Changes in hurricanes from a 13-yr convection-
662 permitting pseudo- global warming simulation. *J. Climate*, **31**, 3643–3657, [https://doi.org/
663 10.1175/JCLI-D-17-0391.1](https://doi.org/10.1175/JCLI-D-17-0391.1).

664 Hausfather, Z., K. Marvel, G. A. Schmidt, J. W. Nielsen-Gammon, and M. Zelinka, 2022: Climate
665 simulations: recognize the ‘hot model’ problem. *Nature*, **605 (7908)**, 26–29.

666 Hersbach, H., and Coauthors, 2020: The era5 global reanalysis. *Quarterly Journal of the Royal
667 Meteorological Society*, **146 (730)**, 1999–2049.

668 Hill, K. A., and G. M. Lackmann, 2011: The impact of future climate change on tc intensity and
669 structure: A downscaling approach. *J. Climate*, **24 (17)**, 4644–4661.

670 Jones, S. C., and Coauthors, 2003: The extratropical transition of tropical cyclones: Forecast
671 challenges, current understanding, and future directions. *Wea. Forecasting*, **18 (6)**, 1052–1092.

672 Jung, C., and G. M. Lackmann, 2019: Extratropical transition of hurricane irene (2011) in a
673 changing climate. *J. Climate*, **32**, 4847–4871, <https://doi.org/10.1175/JCLI-D-18-0558.1>.

674 Jung, C., and G. M. Lackmann, 2021: The response of extratropical transition of tropical cy-
675 clones to climate change: Quasi-idealized numerical experiments. *J. Climate*, **34**, 4361–4381,
676 <https://doi.org/10.1175/JCLI-D-20-0543.1>.

677 Jung, C., and G. M. Lackmann, 2023: Changes in tropical cyclones undergoing extratropical tran-
678 sition in a warming climate: Quasi-idealized numerical experiments of north atlantic landfalling
679 events. *Geophys. Res. Lett.*, **50**, <https://doi.org/10.1029/2022GL101963>.

680 Keller, J. H., and Coauthors, 2019: The extratropical transition of tropical cyclones. part ii:
681 Interaction with the midlatitude flow, downstream impacts, and implications for predictability.
682 *Mon. Wea. Rev.*, **147**, 1077–1106, <https://doi.org/10.1175/MWR-D-17-0329.1>.

683 Kilgore, R., and Coauthors, 2019: Applying climate change information to hydrologic and coastal
684 design of transportation infrastructure. Tech. rep.

685 Kimura, F., and A. Kitoh, 2007: Downscaling by pseudo global warming method. *The Final Report
686 of ICCAP*, **4346**, 463–478.

- 687 Knutson, T., and Coauthors, 2020: Tropical cyclones and climate change assessment part ii:
688 Projected response to anthropogenic warming. *Bull. Amer. Meteor. Soc.*, **101**, E303–E322,
689 <https://doi.org/10.1175/BAMS-D-18-0194.1>.
- 690 Knutson, T. R., J. J. Sirutis, M. A. Bender, R. E. Tuleya, and B. A. Schenkel, 2022: Dynamical
691 downscaling projections of late twenty-first-century u.s. landfalling hurricane activity. *Climatic
692 Change*, **171**, 28, <https://doi.org/10.1007/s10584-022-03346-7>.
- 693 Knutson, T. R., J. J. Sirutis, M. Zhao, R. E. Tuleya, M. Bender, G. A. Vecchi, G. Villarini, and
694 D. Chavas, 2015: Global projections of intense tropical cyclone activity for the late twenty-first
695 century from dynamical downscaling of cmip5/rcp4.5 scenarios. *J. Climate*, **28** (18), 7203–7224.
- 696 Knutson, T. R., and R. E. Tuleya, 2004: Impact of co₂-induced warming on simulated hur-
697 ricane intensity and precipitation: Sensitivity to the choice of climate model and convective
698 parameterization. *J. Climate*, **17** (18), 3477–3495.
- 699 Kourtis, I. M., and V. A. Tsirintzis, 2022: Update of intensity-duration-frequency (idf) curves
700 under climate change: a review. *Water Supply*, **22** (5), 4951–4974.
- 701 Kunkel, K., and Coauthors, 2020: North carolina climate science report. Tech. rep., North Carolina
702 Institute for Climate Studies.
- 703 Lackmann, G. M., 2013: The south-central u.s. flood of may 2010: Present and future*. *J. Climate*,
704 <https://doi.org/10.1175/JCLI>.
- 705 Lackmann, G. M., 2015: Hurricane sandy before 1900 and after 2100. *Bull. Amer. Meteor. Soc.*,
706 **96**, 547–560, <https://doi.org/10.1175/BAMS-D-14-00123.1>.
- 707 Landsea, C. W., and J. L. Franklin, 2013: Atlantic hurricane database uncertainty and presentation
708 of a new database format. *Mon. Wea. Rev.*, **141** (10), 3576–3592.
- 709 Liu, M., G. A. Vecchi, J. A. Smith, and H. Murakami, 2017: The present-day simulation and
710 twenty-first-century projection of the climatology of extratropical transition in the north atlantic.
711 *J. Climate*, **30**, 2739–2756, <https://doi.org/10.1175/JCLI-D-16-0352.1>.

712 Liu, M., G. A. Vecchi, J. A. Smith, and H. Murakami, 2018: Projection of landfalling-tropical
713 cyclone rainfall in the eastern united states under anthropogenic warming. *J. Climate*, **31**, 7269–
714 7286, <https://doi.org/10.1175/JCLI-D-17-0747.1>.

715 Liu, M., L. Yang, J. A. Smith, and G. A. Vecchi, 2020: Response of extreme rainfall for landfalling
716 tropical cyclones undergoing extratropical transition to projected climate change: Hurricane
717 irene (2011). *Earth's Future*, **8**, <https://doi.org/10.1029/2019EF001360>.

718 Livneh, B., E. A. Rosenberg, C. Lin, B. Nijssen, V. Mishra, K. M. Andreadis, E. P. Maurer, and
719 D. P. Lettenmaier, 2013: A long-term hydrologically based dataset of land surface fluxes and
720 states for the conterminous united states: Update and extensions. *Journal of Climate*, **26** (23),
721 9384–9392.

722 Lynch, P., and X.-Y. Huang, 1992: Initialization of the hirlam model using a digital filter. *Mon.*
723 *Wea. Rev.*, **120** (6), 1019–1034.

724 Mallard, M. S., G. M. Lackmann, and A. Aiyyer, 2013a: Atlantic hurricanes and climate change.
725 part ii: Role of thermodynamic changes in decreased hurricane frequency. *J. Climate*, **26** (21),
726 8513–8528.

727 Mallard, M. S., G. M. Lackmann, A. Aiyyer, and K. Hill, 2013b: Atlantic hurricanes and climate
728 change. part i: Experimental design and isolation of thermodynamic effects. *J. Climate*, **26** (13),
729 4876–4893.

730 Michaelis, A. C., and G. M. Lackmann, 2019: Climatological changes in the extratropical transition
731 of tropical cyclones in high-resolution global simulations. *J. Climate*, [https://doi.org/10.1175/
732 JCLI-D-19](https://doi.org/10.1175/JCLI-D-19).

733 Michaelis, A. C., and G. M. Lackmann, 2021: Storm-scale dynamical changes of extratropical
734 transition events in present-day and future high-resolution global simulations. *J. Climate*, **34**,
735 5037–5062, <https://doi.org/10.1175/JCLI-D-20-0472.1>.

736 Miro, M., A. DeGaetano, C. Samaras, K. R. Grocholski, T. López-Cantú, M. Webber, and B. Eck,
737 2021: Projected intensity-duration-frequency (idf) curve tool for the chesapeake bay watershed
738 and virginia. *website*), *Northeast Regional Climate Center*, available online: [https://midatlantic-
739 idf.rcc-acis.org/](https://midatlantic-idf.rcc-acis.org/), last accessed May, **4**, 2022.

740 Moss, R. H., and Coauthors, 2010: The next generation of scenarios for climate change research
741 and assessment. *Nature*, **463 (7282)**, 747–756.

742 National Centers for Environmental Prediction, National Weather Service, NOAA, U.S. Department
743 of Commerce, 2015: Ncep gdas/fnl 0.25 degree global tropospheric analyses and forecast grids.
744 Research Data Archive at the National Center for Atmospheric Research, Computational and
745 Information Systems Laboratory, Boulder CO, URL <https://doi.org/10.5065/D65Q4T4Z>.

746 Nolan, D. S., B. D. McNoldy, and J. Yunge, 2021: Evaluation of the surface wind field over
747 land in wrf simulations of hurricane wilma (2005). part i: Model initialization and simulation
748 validation. *Mon. Wea. Rev.*, **149**, 679–695, <https://doi.org/10.1175/MWR-D-20-0199.1>.

749 Otte, T. L., C. G. Nolte, M. J. Otte, and J. H. Bowden, 2012: Does nudging squelch the extremes
750 in regional climate modeling? *Journal of Climate*, **25 (20)**, 7046–7066.

751 Pasch, R. J., T. B. Kimberlain, and S. R. Stewart, 1999: Preliminary report hurricane floyd. Tech.
752 rep., National Hurricane Center.

753 Peckham, S. E., T. G. Smirnova, S. G. Benjamin, J. M. Brown, and J. S. Kenyon, 2016: Imple-
754 mentation of a digital filter initialization in the wrf model and its application in the rapid refresh.
755 *Mon. Wea. Rev.*, **144 (1)**, 99–106.

756 Pierce, D. W., D. R. Cayan, and B. L. Thrasher, 2014: Statistical downscaling using localized
757 constructed analogs (loca). *J. Hydrometeor.*, **15 (6)**, 2558 – 2585, [https://doi.org/https://doi.org/](https://doi.org/https://doi.org/10.1175/JHM-D-14-0082.1)
758 [10.1175/JHM-D-14-0082.1](https://doi.org/10.1175/JHM-D-14-0082.1).

759 Rappaport, E. N., 2014: Fatalities in the united states from atlantic tropical cyclones: New data
760 and interpretation. *Bull. Amer. Meteor. Soc.*, **95 (3)**, 341–346.

761 Reed, K. A., A. M. Stansfield, M. F. Wehner, and C. M. Zarzycki, 2020: Forecasted attribution of
762 the human influence on hurricane florence. *Science Advances*, **6 (1)**, eaaw9253, [https://doi.org/](https://doi.org/10.1126/sciadv.aaw9253)
763 [10.1126/sciadv.aaw9253](https://doi.org/10.1126/sciadv.aaw9253).

764 Saha, S., and Coauthors, 2010: The ncep climate forecast system reanalysis. *Bull. Amer. Meteor.*
765 *Soc.*, **91 (8)**, 1015–1058.

- 766 Sato, T., F. Kimura, and A. Kitoh, 2007: Projection of global warming onto regional precip-
767 itation over mongolia using a regional climate model. *Journal of Hydrology*, **333**, 144–154,
768 <https://doi.org/10.1016/j.jhydrol.2006.07.023>.
- 769 Schär, C., C. Frei, D. Lüthi, and H. C. Davies, 1996: Surrogate climate-change scenarios for
770 regional climate models. *Geophys. Res. Lett.*, **23**, 669–672, <https://doi.org/10.1029/96GL00265>.
- 771 Seneviratne, S. I., and Coauthors, 2023: *Weather and Climate Extreme Events in a Changing*
772 *Climate*, chap. Climate Change 2021 – The Physical Science Basis, 1513–1766. Cambridge
773 University Press, <https://doi.org/10.1017/9781009157896.013>.
- 774 Skamarock, W. C., and Coauthors, 2019: A description of the advanced research wrf version 4.
775 *NCAR tech. note ncar/tn-556+ str*, **145**.
- 776 Stansfield, A. M., K. A. Reed, and C. M. Zarzycki, 2020: Changes in precipitation from north
777 atlantic tropical cyclones under rcp scenarios in the variable-resolution community atmosphere
778 model. *Geophys. Res. Lett.*, **47**, <https://doi.org/10.1029/2019GL086930>.
- 779 Stewart, S. R., 2017: Hurricane matthew. Tech. rep., National Hurricane Center.
- 780 Stewart, S. R., and R. Berg, 2019: Hurricane florence. Tech. rep., National Hurricane Center.
- 781 Tokarska, K. B., M. B. Stolpe, S. Sippel, E. M. Fischer, C. J. Smith, F. Lehner, and R. Knutti,
782 2020: Past warming trend constrains future warming in cmip6 models. *Science Advances*, **6** (12),
783 eaaz9549, <https://doi.org/10.1126/sciadv.aaz9549>.
- 784 Trapp, R. J., and K. A. Hoogewind, 2016: The realization of extreme tornadic storm events
785 under future anthropogenic climate change. *J. Climate*, **29**, 5251–5265, <https://doi.org/10.1175/JCLI-D-15-0623.1>.
- 787 von Storch, H., H. Langenberg, and F. Feser, 2000: A spectral nudging technique for dynamical
788 downscaling purposes. *Mon. Wea. Rev.*, **128** (10), 3664–3673.
- 789 Waldron, K. M., J. Paegle, and J. D. Horel, 1996: Sensitivity of a spectrally filtered and nudged
790 limited-area model to outer model options. *Mon. Wea. Rev.*, **124** (3), 529–547.

791 Wright, D. B., C. D. Bosma, and T. Lopez-Cantu, 2019: Us hydrologic design standards insufficient
792 due to large increases in frequency of rainfall extremes. *Geophysical Research Letters*, **46** (14),
793 8144–8153.

794 Wright, D. B., T. R. Knutson, and J. A. Smith, 2015: Regional climate model projections of rainfall
795 from u.s. landfalling tropical cyclones. *Climate Dynamics*, **45**, 3365–3379, [https://doi.org/10.](https://doi.org/10.1007/s00382-015-2544-y)
796 1007/s00382-015-2544-y.